ACS APPLIED MATERIALS & INTERFACES

www.acsami.org

Research Article

Interfacial Polymerization of Aromatic Polyamide Reverse Osmosis Membranes

Size Zheng, Jacob Gissinger, Benjamin S. Hsiao,* and Tao Wei*

Cite This: *ACS Appl. Mater. Interfaces* 2024, 16, 65677−65686

Read Online

ACCESS | Metrics & More | Article Recommendations | Supporting Information

ABSTRACT: Polyamide membranes are widely used in reverse osmosis (RO) water treatment, yet the mechanism of interfacial polymerization during membrane formation is not fully understood. In this work, we perform atomistic molecular dynamics simulations to explore the cross-linking of trimesoyl chloride (TMC) and m-phenylenediamine (MPD) monomers at the aqueous−organic interface. Our studies show that the solution interface provides a function of "concentration and dispersion" of monomers for cross-linking. The process starts with rapid cross-linking, followed by slower kinetics. Initially, amphiphilic MPD monomers diffuse in water and accumulate at the solution interface to interact with TMC monomers from the organic phase. As cross-linking progresses, a precross-linked thin film forms, reducing monomer diffusion and reaction rates. However, the structural flexibility of the amphiphilic film, influenced by interfacial fluctuations and mixed interactions with water and the organic solvent at the solution interface, promotes further cross-linking. The solubility of MPD and TMC monomers in different organic solvents (cyclohexane *versus* *n*-hexane) affects the cross-linking rate and surface homogeneity, leading to slight variations in the structure and size distribution of subnanopores. Our study of the interfacial polymerization process in explicit solvents is essential for understanding membrane formation in various solvents, which will be crucial for optimal polyamide membrane design.

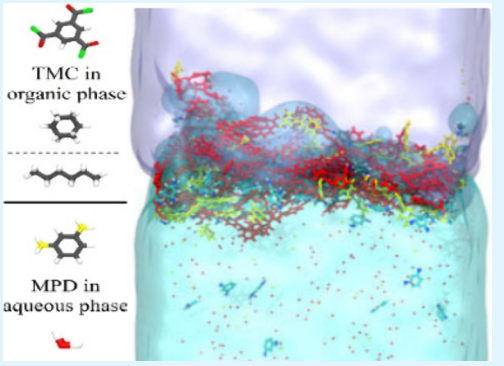

KEYWORDS: *Interfacial Cross-linking, Polymerization, Polyamide Membrane, Atomistic Molecular Dynamics Simulations, Solvent Effect*

1. INTRODUCTION

The process of preparing drinking water from seawater and brackish water involves many stages, where the final and most expensive stage is typically reverse osmosis (RO). In RO, water is forced through a semipermeable membrane under pressure that exceeds the osmotic pressure of the feed solution. This pressure-driven process separates water from dissolved ions and impurities, resulting in purified water. The rate at which water passes through the membrane, known as the water flux, is proportional to the applied pressure, while the energy consumption of the process depends on the total pressure applied. The critical component of RO membranes is a thin, nanoporous amorphous polyamide layer, typically on the order of hundreds of nanometers in thickness. This layer is created through interfacial polymerization (IP), which involves reacting m-phenylenediamine (MPD) and trimesoyl chloride (TMC) in two immiscible solution (aqueous and organic) phases, resulting in a heterogeneously cross-linked amorphous film with nanoscale pores essential for filtration. The IP approach to prepare thin polyamide films was demonstrated by Mogan first in 1965,[1] and Cadotte later used this method to create the polyamide barrier layer on a microporous support, forming thin film composite (TFC) RO membranes in 1976.[2] Cadotte's method sparked significant industrial and academic interests, leading to the commercialization of TFC membranes for RO applications.[3] However, some challenges remain to fabricate the IP cross-linked membrane with high performance, i.e., maintaining high water flux and high salt rejection capability simultaneously, at low energy production cost. A fundamental understanding of the molecular mechanism of the IP process is thus critical to future membrane design and fabrication.

The IP process consists of the diffusion of monomers in solvent and cross-linking reactions at the aqueous−organic interface. Solvent composition at the solution interface is crucial to the orientation, distribution, and structure of monomers and surfactants during IP. At the microscopic level, an interface between two immiscible solutions exhibits thermal fluctuations, which inevitably affects the stability of the cross-linked network and the formation of a uniform thin film. Experiments have demonstrated that the solution environment can also affect the cross-linking process, altering the microscopic structure and performance of the resulting polyamide

Received: September 22, 2024
Revised: November 10, 2024
Accepted: November 13, 2024
Published: November 18, 2024

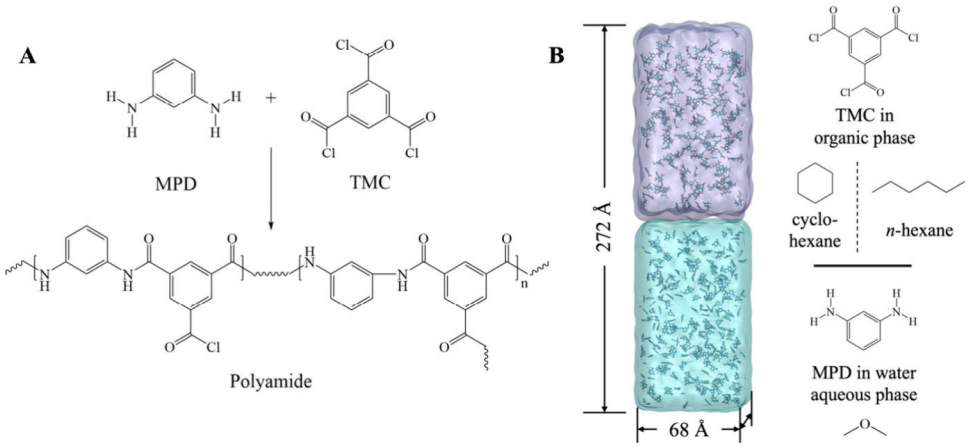

Figure 1. Configuration of MD simulation. (A) Structure formula of MPD and TMC monomers and the cross-linked polyamide. (B) Initial setup of the simulation systems. The top purple section is the organic phase consisting of either *n*-hexane or cyclohexane, while the bottom blue section is the aqueous phase.

barrier layer.[4−8] The use of organic solvents, such as *n*-hexane, cyclohexane, heptane and isopar, was found to influence water permeation, primarily by affecting MPD diffusivity and solubility during MPD−TMC thin film cross-linking.[4] The addition of poly(vinyl alcohol) to the aqueous phase was shown to reduce monomer diffusion, resulting in membranes with a Turing structure, characterized by more corrugation, voids, and islands, which can enhance water desalination.[5] Incorporating ionic liquid molecules into the IP could alter the membrane's microscopic structure and improve the desalination performance, including permeate flux and salt rejection ratio.[6] It was also found that the addition of surfactants accelerates MPD diffusion into the organic phase resulting in a more complete IP reaction.[9]

Atomistic molecular dynamics (MD) simulations offer significant insights into atomic-scale details and dynamics from subnanosecond to microsecond regimes, complementing experimental developments.[10−22] To achieve water-salt separation and selectivity, the majority of pores in polyamide membranes have diameters at the subnanometer scale, which needs high-resolution atomistic simulations.[13,23] Moreover, the intricate microscopic structure of the polyamide also demands high-resolution simulations. The molecular backbone packing of the polyamide membrane features two aromatic packing motifs: parallel ($\pi-\pi$ stacking) and perpendicular (T-shaped).[24,25] Extensive atomistic MD simulations have previously been conducted to establish cross-linked polyamide membranes, in which cross-linking reactions were performed in a vacuum, particularly at high temperature, to ensure a full structural relaxation during cross-linking.[13,14,18,26−29] Monte Carlo approaches with random walks have also been adopted to generate cross-linked polymer networks in vacuum.[19] Alternative Langevin simulations with coarse-grained (CG) models in implicit solvent have been applied to study the IP process.[30]

Despite immense progress in experiments,[3−9,23,25,31−38] theoretical simulations[12−14,18,29,39−41] and machine learning[26,42−44] for polyamide RO membranes, the effects of the solution on monomer diffusion and cross-linking reactions in the solution interface at the microscopic scale remain unclear. The absence of explicit solvents in previous simulation studies has limited the ability to accurately represent the solution interface and its impact on the IP process.[13,14] The goal of this work is to study the molecular mechanism of the IP process at the aqueous−organic interface and the microscopic structure (heterogeneity and orientation of aromatic rings) of the polyamide thin film in different solvent environments using large-scale atomistic MD simulations. To understand the IP process, we perform explicit solvents in our atomistic MD simulations. Specifically, we focus on the initial period of the IP (less than 1.0 μs), which plays a key role in forming the cross-linked polymer membrane. This stage involves monomer diffusion and reactions at the solution interface, and also the development of a thin membrane (only a few nanometers thick) that fully covers the surface at the aqueous−organic interface. The thin film at the solution interface lays down the structural framework for further cross-linking and the development of a membrane with greater thickness.

In our simulations, we use the software of LAMMPS (Large-scale Atomic/Molecular Massively Parallel Simulator), which enables the creation of chemical bonds between neighboring reaction-active sites.[45−49] In our simulations, MPD monomers are initially dispersed in water, while both linear *n*-hexane and ring-shaped cyclohexane are used as organic solvents to dissolve TMC monomers. Our simulations provide new insights into the critical role of "concentration and dispersion" of monomers at the solution interface for cross-linking. In addition to the study of the IP process, we characterize the structure of the cross-linked polyamide membrane and compare it to the previous studies to validate the reliability of our simulations.[4,13,14] Our study of the IP process in an explicit solvent environment is crucial for understanding experimental measurements involving different solvent environments. This new knowledge will facilitate rational design of cross-linked polyamide membranes for various applications in water and gas separation.

2. EXPERIMENTAL SECTION

Atomistic MD simulations of the IP process are conducted using LAMMPS software.[45] The OPLS-AA force field, commonly used in polymer simulations (including polyamide membranes)[50−53] is employed in our simulations. To simulate the condensation reactions for the formation of a cross-linked polyamide structure (Figure 1A), we employ the REACTOR protocol to model predetermined topology changes through standard force fields.[46−49] This approach involves defining topology changes in pre- and post-reaction molecule templates, including the creation and deletion of bonds, angles,

https://doi.org/10.1021/acsami.4c16229
ACS Appl. Mater. Interfaces 2024, 16, 65677−65686

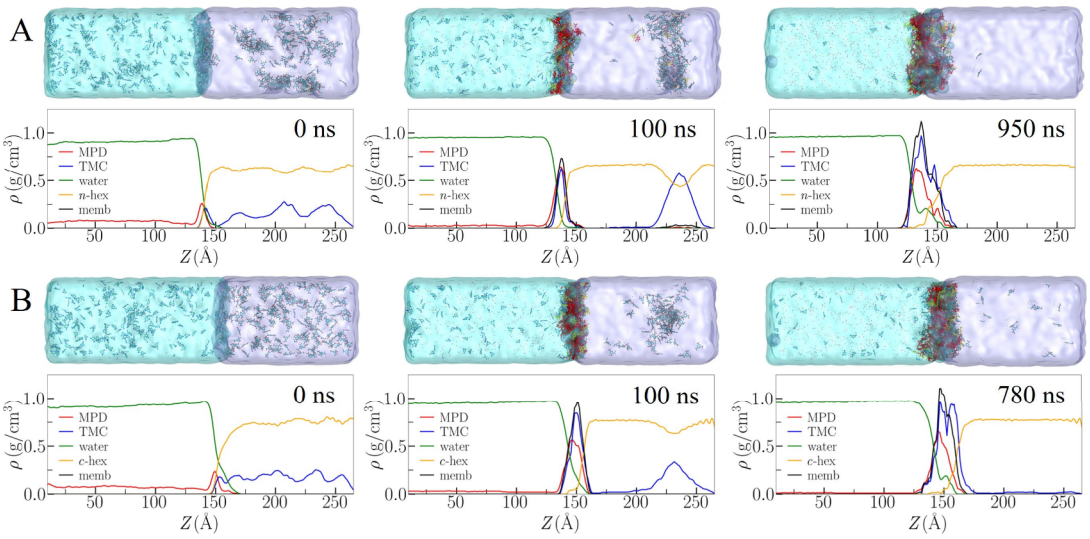

Figure 2. Cross-linking process of polyamide thin films. Representative snapshots and corresponding density profiles of (A) *n*-hexane and (B) cyclohexane systems are shown at key time points, respectively. Fully cross-linked monomers are depicted in red and partially cross-linked monomers in yellow. TMC aggregates are observed in both systems at 100 ns. Final membrane densities (approximately 1.2 g/cm^3) are consistent with experimental measurements (1.1−1.3 g/cm^3). "*n*-hex", "*c*-hex", and "memb" in the legends represent *n*-hexane, cyclohexane, and membrane, respectively.

dihedrals, and improper dihedrals, as well as alteration of atomic partial charges. Molecular connectivity, atomic partial charges, and the intra- and intermolecular interactions are updated after the cross-linking (see Figure S1 and Table S1 in the Supporting Information), which circumvents the need for quantum mechanical or pairwise bond-order potential methods, thereby enabling significantly larger system sizes and faster simulation speeds. Therefore, we can investigate the entire IP process at large temporal and spatial scales, including explicit solvents.

Previous experimental studies[54−56] showed that the MPD/TMC condensation reaction is much faster than the reaction of TMC hydrolysis. Since the goal of this study is to examine the crucial initial period of film formation within the first microsecond, we ignore the rare events of hydrolysis and focus only on condensation reactions at the aqueous−organic interface in our simulations. The condensation reaction between MPD and TMC involves the breakage of two covalent bonds—specifically, the N−H and C−Cl bonds—resulting in the formation of a new amide linkage (Figure 1A and Figure S1 in the Supporting Information). In our simulations, the condensation reaction is governed by the criterion that a nitrogen atom within the amino group of MPD and a carbon atom within the acyl chloride group of TMC must be unreacted and within a cutoff distance of 5.0 Å. This chosen cutoff is small enough to allow for relaxation of the reacting molecules while also being large enough to achieve satisfactory cross-linking degrees.[47] The degree of polymer cross-linking (DPC) is defined by the percentage of fully reacted TMC, where all three amine groups have reacted with MPD monomers, relative to the initial total number of TMC in the system (Figure 1A).[13,14]

In this study, two simulation systems are constructed, respectively, for the *n*-hexane and cyclohexane systems, as shown in Figure 1B. Molecular models of MPD, TMC, *n*-hexane and cyclohexane are constructed using Moltemplate scripts, which also assigns the topology information and force field parameters.[57] Water molecules are represented using the TIP3P model. In both systems, a simulation box with a total dimension of 68 × 68 × 272 Å^3 is divided into two phases. The aqueous phase contains 300 MPD monomers and 19,488 water molecules, with a weight percent of 8.5%. The organic phase contains 200 TMC monomers and 2,606 cyclohexane/*n*-hexane molecules, with a weight percentage of approximately 19%. Due to the inherent size limitations of MD simulations, the concentrations of MPD and TMC in our simulations are much higher than experimental values (typically 0.1% MPD and 0.04% TMC) to ensure a sufficient number of monomers with the same molar ratio as in the experiment having adequate membrane thickness. Periodic boundary conditions are applied along the *X*- and *Y*-axes, while fixed boundaries are assigned to the *Z*-axis. To prevent particles from escaping, purely repulsive implicit walls are established at both the top and bottom boundaries. The addition of an implicit wall has negligible effects on the solution interface because our system has sufficient length (13.6 nm) in each phase. However, it effectively separates the organic and aqueous phases, allowing monomers to react only at a single solution interface and enabling the formation of a membrane with sufficient thickness. van der Waals interactions are modeled using the Lennard-Jones potential with a cutoff distance of 1.2 nm. Long-range electrostatic interactions are calculated using the Particle−Particle Particle-Mesh (PPPM) solver.[58] After system construction, equilibration runs are initially conducted in the NVT ensemble for 2 ns, followed by NPT runs for an additional 3 ns. The system temperature is maintained at 300 K using the Nosé−Hoover thermostat, while the pressure is kept at approximately 1.0 atm using the Nosé−Hoover barostat.[59−62] During the initial equilibration, monomers freely diffuse within and between phases, while the cross-linking reactions remains temporarily inactive. The reaction simulations are then performed at 300 K for 950 and 780 ns for the *n*-hexane and cyclohexane systems, respectively, until the temporal DPC curves reach plateaus. The simulations apply a time step of 1 fs. The cross-linking reactions are evaluated every 100 fs, with only one MPD-TMC pair selected per evaluation to prevent simultaneous bond formation between adjacent monomers. The H^+ and Cl^- ions generate from the condensation reactions are retained in the system and allowed to diffuse freely.

3. RESULTS AND DISCUSSION

3.1. Cross-Linking Dynamics. To investigate the IP process, which involves the complex coupling of chemical reactions and monomer diffusion, we perform atomistic MD simulations using explicit solvents. Monomers of MPD and TMC are first dispersed in the water phase and the organic phase (either *n*-hexane or cyclohexane), respectively. Before performing the cross-linking simulations, a short equilibration simulation lasting 5 ns is conducted to allow the simulation system to relax. As shown in the density profiles of solvents and monomers in Figure 2, the aqueous−organic interface is

https://doi.org/10.1021/acsami.4c16229
ACS Appl. Mater. Interfaces 2024, 16, 65677−65686

located at approximately 130 Å < z < 170 Å. As the cross-linking simulation proceeds, MPD and TMC monomers continue diffusing to the solution interface, where they react with each other, forming a three-dimensional cross-linked film that increases the polymer density at the interface. By the end of the simulations (950 ns for the *n*-hexane system and 780 ns for the cyclohexane system), the highest-density regions of the cross-linked thin layers exceed 1.2 g/cm^3 (Figure 2), which is within the experimental range (1.1−1.3 g/cm^3).[63]

During the IP process, TMC monomers aggregate in the bulk organic phase (Figure 2A and 2B). This observation agrees with experiments, which show that TMC monomers have low solubility and are prone to aggregation.[64] In experiments, monomers are usually dispersed by ultrasound before initiating cross-linking to prevent aggregation. In our simulations, the concentrations of monomers are much higher than that in experiments to reduce computational load, which can result in increased TMC aggregation in the organic phase.[65] In cyclohexane, the TMC aggregates eventually dissolve, and the TMC monomers can gradually diffuse to the solution interface and participate in the cross-linking reaction with the thin film (Figure 2A and Figure S2A in the Supporting Information). However, in *n*-hexane, the TMC aggregates are more stable and eventually diffuse to the solution interface, where they react with the unreacted sites of the thin film and become part of it (Figure 2B and Figure S2B in the Supporting Information). It is notable that throughout the entire course of IP, a small overlap in the density profiles of water and the organic solvent (*n*-hexane or cyclohexane) at the solution interface indicates mixing of the solvents, even though the solution interface is present (Figure 2). Additionally, during the process of the IP, water or organic droplets form near the solution interface and diffuse to the opposite phase (Figure 3), introducing significant heterogeneity in the molecular dispersion at the solution interface, even though the aqueous−organic interface remains present throughout the cross-linking process (Figure 2). As discussed later, the mixing of solvent molecules at the solution interface causes variations of solvent interactions with the amphiphilic polyamide thin film and increases the structural flexibility of the precross-linked film, promoting further polymer cross-linking at the solution interface.

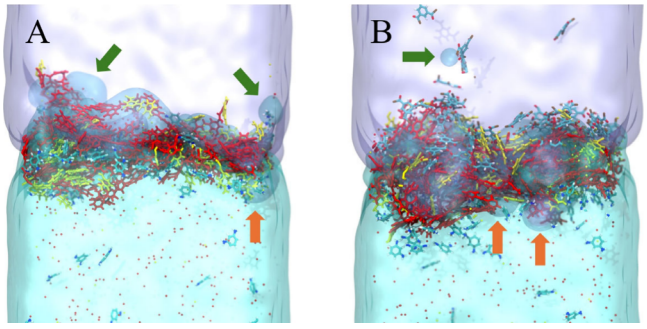

Figure 3. Snapshots of the (A) *n*-hexane and (B) cyclohexane systems at 500 ns, showing water and oil droplets forming in the opposite phase. The blue background represents the water phase (bottom), while the purple color indicates the organic phase (top). The red beads in the water phase represents the H^+ and Cl^- ions produced during the condensation reaction. The green arrows point to the water droplets in the oil phase, while the orange arrows indicate the oil droplets in the aqueous phase.

Figure 4A illustrates the temporal evolution of the DPC throughout the simulation, demonstrating the rate of monomer condensation. The cross-linking process clearly exhibits distinct stages: an initial rapid cross-linking stage followed by one or more slower stages (Figure 4A). For cyclohexane, the cross-linking reactions slow down after around 50 ns, while for *n*-hexane, the first slowdown occurs after approximately 40 ns, with another slowdown observed after around 600 ns (Figure 4A). To more precisely quantify the condensation reaction rate, we also monitor the total number of bonds formed throughout the entire process (see Figure S3 in the Supporting Information), including reactions not counted in the DPC definition. The temporal profiles of the total number of amide bonds for both cyclohexane and *n*-hexane show trends similar to those of the DPC temporal profiles. Our simulation agrees with the experimental studies, which also shows a decrease in the cross-linking rate after the initial stage of fast reactions.[66] The initial IP process is very fast due to the rapid accumulation of MPD at the solution interface and the high reactivity of the monomers. Subsequently, the reaction rate decreases significantly as the forming polyamide layer impedes monomer diffusion toward the interface due to steric effects of the precross-linked thin film, slowing further interactions between monomers or between monomers and unreacted sites on the film. As the cross-linked structure develops, the number of uncross-linked reactive sites decreases, and those sites buried within the thin film become less likely to react with each other. Additionally, the decrease in the concentrations of MPD and TMC in the bulk solution also affects the reaction rate. Further discussion will be provided in the following sections.

Notable differences in the cross-linking rates during the second stage are observed between the two systems (Figure 4A). After the initial stage, the *n*-hexane system maintains an almost linear cross-linking rate until approximately 600 ns, ultimately achieving about 25% higher DPC than the cyclohexane system at 750 ns. The faster cross-linking rate and the two slowdowns observed in the case of *n*-hexane, compared to cyclohexane, can be explained by examining the 2D density maps of the polyamide thin layer in the *X*-*Y* plane at the solution interface (120 Å < z < 180 Å), shown in Figure 4B and 4C. Compared to the thin film at the water-cyclohexane interface at 50 ns, the density of the thin film initially formed at the water-*n*-hexane interface at the same time is more heterogeneous. This indicates that the initial coverage of the thin film at the water-*n*-hexane interface is incomplete, facilitating the diffusion of monomers and supporting continued cross-linking reactions. Moreover, until the cross-linked thin film fully covers the interface at approximately 780 ns (Figure 4B), the cross-linking reaction rate for *n*-hexane reaches a plateau (Figure 4A). Additional density maps illustrating the progression of the cross-linking process for both systems are provided in Figure S4 in the Supporting Information. The variation in cross-linking rates is attributed to the differing solubility of TMC in the organic solvents. The higher tendency of TMC to aggregate in *n*-hexane can impede continuous monomer diffusion to the interface, resulting in a relatively slower initial cross-linking rate and incomplete formation of the polyamide thin layer. The water-*n*-hexane interface is not fully covered before 600 ns, during which the reaction rate remains linear. After 600 ns, the reaction rate gradually decreases until reaching a plateau at approximately 780 ns, due to the steric hindrance at the jamming limit of molecular packing.

https://doi.org/10.1021/acsami.4c16229
ACS Appl. Mater. Interfaces 2024, 16, 65677−65686

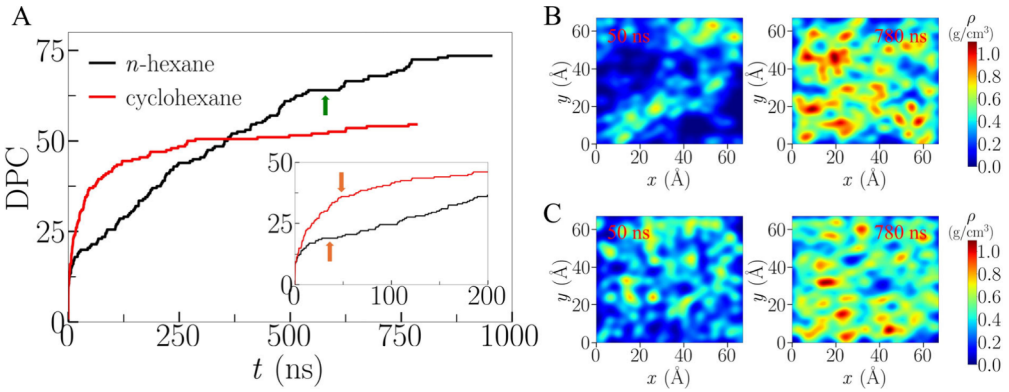

Figure 4. Cross-linking dynamics and density distributions in the *n*-hexane and cyclohexane systems. (A) Temporal evolution of the DPC. Orange arrows in the inset indicate transition points between the initial rapid cross-linking stage and the extended slow kinetics phase, while the green arrow denotes the second deceleration in the cross-linking process. The cyclohexane system shows a steeper initial DPC increase rate but achieves a lower final DPC compared to the *n*-hexane system. (B and C) Density maps of *n*-hexane and cyclohexane systems, respectively, at the solution interface near the end of the first stage (50 ns, left) and the end of the entire simulations (780 ns, right). The images are smoothed using Gaussian blur.

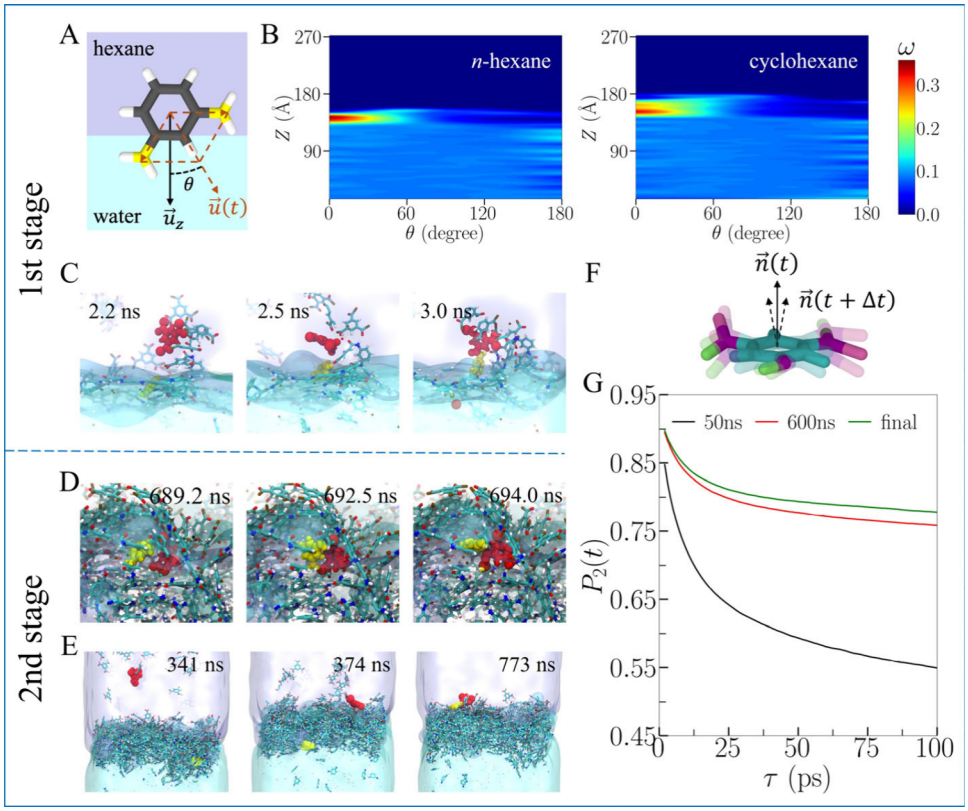

Figure 5. Dynamics analysis of the two-stage cross-linking process. (A) Schematic representation of the calculation of orientation angle θ. (B) Two-dimensional orientation distribution $\omega(z,\theta)$ of MPD monomers at the interface between water and *n*-hexane (left) or cyclohexane (right) phases before the initiation of reactions. In both systems, MPD monomers oriented their $\vec{u}(t)$ vectors toward the negative *Z*-axis at the solvent interface. (C-E) Representative snapshots of the cyclohexane system illustrating the stages of the cross-linking reaction (red: TMC, yellow: MPD): (C) Rapid initial cross-linking of TMC and MPD molecules at the interface during the first stage. (D) Slow cross-linking between the uncross-linked sites of cross-linked monomers within the polyamide thin layer. (E) Slow cross-linking between partially cross-linked monomers of the polyamide thin layer and monomer diffusing from the bulk. (F) Schematic diagram of reorientation dynamics calculation of cross-linked backbones. $\vec{n}(t)$ is the vector normal to the benzene ring's planes. (G) Backbone reorientation dynamics of benzene rings, $P_2(t)$, in the cross-linked thin layer, demonstrating the evolution of flexibility of the cyclohexane system through the initial to final time of the simulation.

The accumulation and conformations of monomers at the interface prior to cross-linking reactions play a crucial role in the subsequent polymerization process and ultimately influence the structural characteristics of the formed polyamide thin layer. Due to the distinct hydrophobicity at the interface, MPD, being an asymmetric amphiphilic molecule, exhibits preferential orientation. To quantify the orientation preference at the solution interface, we analyze the distribution of MPD orientations using the two-dimensional orientation distribution function $\omega(z,\theta)$ as follows,[15,67]

https://doi.org/10.1021/acsami.4c16229
ACS Appl. Mater. Interfaces 2024, 16, 65677−65686

$$\omega(z, \theta) = \frac{\langle \delta(\theta - \theta(t))\delta(z - z(t))\rangle}{\rho(z)\sin\theta} \quad (1)$$

where z is the coordinate of the center of mass of MPD monomers along the Z-axis normal to the interface, $\theta(t)$ is the angle between the vector $\vec{u}(t)$, defined by two neighboring amino groups ($-NH_2$) on the benzene ring of MPD, and the negative Z-axis at different times t (Figure 5A), $\delta(\cdots)$ is the Dirac delta function of $\theta(t)$ with respect to (θ in the grid on the 2D density map, and $\langle\cdots\rangle$ represents the ensemble average over all MPD monomers at the solution interface for configurations at different times. Figure 5B shows the analyses of the MPD monomers after the initial relaxation without cross-linking. In the bulk water (z < 130 Å), MPD molecules exhibit random orientations with θ values spanning 0 to 180 deg (Figure 5B). In the organic phase (z > 170 Å), only a few MPD monomers present with random orientation distribution (Figure 5B). However, at the solution interface (130 Å < z < 170 Å), MPD monomers adopt a preferential alignment, with hydrophilic amine groups oriented toward the aqueous phase and hydrophobic benzene rings toward the organic phase (Figure 5B). The ordered structure of the MPD monomer at the aqueous−organic interface is attributed to its amphiphilic nature (i.e., the coexistence of a hydrophilic amine group and a hydrophobic benzene ring). Such ordered alignment finally disappears at the end of the simulations for both systems after polyamide thin layer formed at the solution interface (see Figure S5 in the Supporting Information). Further investigation will focus on the effect of the alignment of the isomers of aromatic diamines (o-phenylenediamine (OPD) and p-phenylenediamine (PPD)) at the aqueous−organic interface on the structure and performance of the polymer membrane in our future studies.[68] The differences in the position of the amino ($-NH_2$) groups on the benzene ring for aromatic diamines (MPD, OPD, and PPD) are expected to lead to different orientations at the aqueous−organic interface, which can affect their distribution at the solution interface and alter the cross-linked structure during the initial stage of cross-linking. Moreover, the addition of surfactants and ionic liquids also changes the interfacial and bulk properties, as well as the distribution and diffusivity of monomers.[5,68] This study can lay the groundwork for further research to provide an in-depth explanation of the experimental results in the future.

We use the case of cyclohexane as an example to illustrate the IP process (Figure 5C to 5E), since both cyclohexane and n-hexane display similar general trends. In the initial rapid reaction stage (t < 50 ns), the absence of a thin film at the interface allows MPD and TMC monomers to diffuse freely, initiating cross-linking (Figure 5C). As a cross-linked thin layer forms, covering the aqueous−organic interface, it creates a steric barrier to advance the cross-linking reaction. This significantly slows down the subsequent cross-linking process, which is essential for the full development of a cross-linked polyamide membrane with sufficient thickness. During the prolonged slow cross-linking process, uncross-linked or partially cross-linked sites within the film can still cross-link with each other (Figure 5D). Reactive sites initially buried within the membrane can dynamically shift to the surface due to large structural rearrangements of the membrane, allowing further cross-linking with monomers from the bulk solution (Figure 5E). To understand the driving force underlying these microscopic dynamics in the slow cross-linking process, we investigate the structural stability of the cross-linked backbone in the polyamide thin film using the third term of the Legendre polynomial $P_2(t)$,[69] which describes the time-dependent molecular reorientation of aromatic rings,

$$P_2(t) = \frac{3\langle(\vec{n}(t + \Delta t)\cdot\vec{n}(t))^2\rangle - 1}{2} \quad (2)$$

where $\vec{n}(t)$ is defined as a unit vector normal to the plane surface of an aromatic ring in the cross-linked film at time t, while $\vec{n}$ $(t + \Delta t)$ is the unit vector normal to the same aromatic ring after a time interval Δt (Figure 5F). The rate at which $P_2(t)$ decays to zero indicates the flexibility of the entire cross-linked film. Figure 5G shows that the $P_2(t)$ profiles of the cyclohexane system exhibit a rapid decay at the first stage. This suggests that the initial precross-linked structure at the solution interface undergoes significant structural fluctuations, making the reactive sites in the membrane more readily available for cross-linking. The fast decay in $P_2(t)$ in the second stage (Figure 5G) is consistent with the microscopic dynamics shown in Figure 5D and 5E. Driven by the phase equilibrium and thermal motion, water and n-hexane or cyclohexane molecules experience large fluctuations at the aqueous−organic interface. Moreover, the cross-linked backbone of the polyamide thin film contains hydrophobic aromatic rings and hydrophilic amide groups, each with different affinities for water and n-hexane or cyclohexane. The large thermal motion at the aqueous−organic interface and the differences in interactions between the hydrophobic and hydrophilic components (i.e., hydrophilic amide groups and hydrophobic aromatic rings) of the membrane with the mixed water and organic solvents at the solution interface result in considerable structural flexibility, which promotes the dispersion of reactive sites for cross-linking. Comparison of the $P_2(t)$ profiles at different times during the prolonged cross-linking shows that as time progresses, the cross-linking degree of the entire structure increases, and the decay of $P_2(t)$ becomes slower (Figure 5G).

The cross-linked polymer membrane has high conformational entropy due to the mixing of different segments within the network, which creates a variety of spatial arrangements. More importantly, as shown in our study, the interfacial fluctuations (i.e., fluctuations in water/hexane molecular distribution, see Figure 2 and 3) and variations in molecular interactions with mixed solvents (water and cyclohexane/n-hexane) result in high structural flexibility of the precross-linked amphiphilic film (Figure 5G) at the solution interface. This structural flexibility enhances cross-linking at reactive sites within the film or between these sites and the monomers from the bulk solution in the prolonged slow cross-linking process. Our analysis of the entire interfacial polymerization process highlights the crucial role of concentration and dispersion of monomers at the aqueous−organic interface for polyamide cross-linking. This interface concentrates monomers at the solution interface in the initial stage to enable rapid cross-linking and later disperses active sites in the cross-linked film, facilitating further cross-linking as the process continues.

3.2. Structures of the Cross-Linked Polyamide Membrane. The local structures of the cross-linked thin layer, primarily determined by the interactions between the benzene groups of bonded and nonbonded monomers, are characterized using order parameter $S(r)$ and radial density ρ_r calculations. Figure 6A illustrates the schematic diagram for these calculations, where r is the radial distance between the centers of mass of the benzene rings, and $\theta(r)$ is the angle

https://doi.org/10.1021/acsami.4c16229
ACS Appl. Mater. Interfaces 2024, 16, 65677−65686

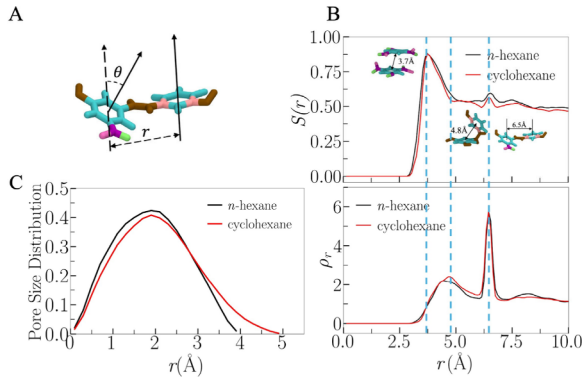

Figure 6. Characterization of the cross-linked polyamide thin layer. (A) Schematic diagram of the order parameter calculation: r is the radial distance between the centers of mass of benzene rings, and $\theta(r)$ is the angle between the normal vectors of neighboring benzene rings at r. (B) Order parameter $S(r)$ and radial density ρ_r profiles of neighboring monomers. Three representative structures are identified: $\pi-\pi$ parallel-stacked rings at $r \approx 3.7$ Å, T-shaped rings at $r \approx 4.8$ Å, and regularly bonded rings at $r \approx 6.5$ Å. The peaks in $S(r)$ and ρ_r profiles show strong correlations. (C) Pore size distribution profiles for n-hexane and cyclohexane systems. Both systems exhibit similar peak pore sizes at $r \approx 2.0$ Å, but the cyclohexane system demonstrates a wider pore size distribution.

between the normal vectors of neighboring benzene rings at r. $S(r)$ is defined by the following equation,

$$S(r) = \left\langle \frac{3\cos^2(\theta(r)) - 1}{2} \right\rangle \tag{3}$$

where $S(r) = 0$ corresponds to a random structure and $S(r) = 1$ represents a completely ordered packing. The relative local density of benzene rings, ρ_r, is determined by Equation 4,

$$\rho_r = \frac{\rho(r)}{\rho_{\text{bulk}}} \tag{4}$$

where ρ_r is the benzene ring density at r, and the bulk density ρbulk is defined as $r > 12$ Å.

As shown in Figure 6B, the $S(r)$ profiles reveal sharp peaks at $r \approx 3.7$. Å, corresponding to $\pi-\pi$ stacking structure, and smaller peaks at $r \approx 6.5$ Å, attributed to regularly bonded benzene rings. Notably, the $S(r)$ of the cyclohexane system is consistently lower than that of the n-hexane system across the investigated distance range, indicating a less ordered overall structure of cross-linked thin layer in the cyclohexane system. The radial density profiles ρ_r show high peaks at $r \approx 6.5$ Å, aligning well with the $S(r)$ profile, and demonstrate that the majority of local structures in the cross-linked thin layers are covalently bonded rings with a slightly torsional angle. Another peak observed at $r \approx 4.8$ Å corresponds to T-shaped rings[13] with the cyclohexane system exhibiting a higher density in this region compared to that of n-hexane (Figure 6B). This suggests more bent structures within the formed thin layer, which results in a larger pore size in the cyclohexane system (Figure 6C). Both systems display a distribution peak at $r \approx 2.0$ Å, which is critical for water-salt separation and is consistent with both experimental and simulation observations.[13,14,23] However, the cyclohexane system's curve shows a lower distribution in the small size range and a wider distribution in the large size range, corroborating the presence of more bent structures within its formed thin layer. The pore size distribution of the polyamide membrane in our study is slightly broader, compared to previous measurements in the literature, due to the thinner layer of the polyamide membrane.[13,14,23] In our measurement of membrane pore size distribution, a larger surface area with larger pores of the thin film is included because of limited data.

It is noteworthy that our simulation, which covers a time scale close to 1.0 μs, does not account for the slow hydrolysis reactions of TMC in water or the heat released during bond breaking.[54,55,70] To reduce the intensive computational load, the monomer concentrations in our simulation are also higher than those applied in the experimental conditions, leading to increased monomer aggregation in the bulk solution. Nevertheless, in comparison to previous experimental measurements, our simulations of interfacial cross-linking involving explicit solvents provide consistent results.[4,23,25] Our simulations elucidate three main structural components (neighboring bonded benzene rings and $\pi-\pi$ conformations (parallel stacking and T-shape)), which are detected in the experiments.[25] Due to computational limitations, the simulated membrane has a thickness (~5 nm) much less than that of the membrane fabricated in experiments; however, the overall pore size distribution is in agreement with experimental measurement.[23] The relatively wider pore size distribution observed in the case of cyclohexane compared to the n-hexane system is also consistent with the experiments, which showes a larger water flux for a polyamide membrane cross-linked in cyclohexane than in n-hexane.[4]

4. CONCLUSIONS

Understanding solvent effects on cross-linking and microscopic dynamics can guide the design of high-performance membranes for many industry applications. In this study, we conduct atomistic MD simulations to investigate the cross-linking process of MPD and TMC with explicit solvents. Our study shows that the solution interface acts as a mechanism for concentrating and dispersing monomers, which is critical for developing a 3D cross-linked membrane structure. The IP process consists of an initial rapid cross-linking stage followed by slower kinetics. The aqueous−organic interface accumulates monomers during the initial stage of cross-linking and disperses active sites in the precross-linked film to promote further cross-linking in the extended period. The initial rapid cross-linking is governed by molecular diffusion. Amphiphilic MPD monomers diffuse to the solution interface, forming an ordered structure at the aqueous−organic interface to interact with TMC monomers. During subsequent slow cross-linking, the solution interface is covered by a precross-linked thin film, which significantly reduces monomer diffusion and reaction rates at the interface. However, the cross-linked backbone of the polyamide thin film, consisting of hydrophobic aromatic rings and hydrophilic amide groups, exhibits large structural fluctuations that promote further 3D cross-linking. Interfacial fluctuations in water/hexane molecular distribution and variations in molecular interactions with mixed solvents lead to high structural flexibility in the precross-linked amphiphilic film. This flexibility enhances cross-linking among the reactive sites within the thin film, or among the uncross-linked or partially cross-linked sites in the film and the monomers from the bulk solution during prolonged cross-linking.

Our study shows that different organic solvents affect cross-linking kinetics and the microscopic structure of the polyamide membrane. Compared to n-hexane, TMC monomers aggregate

https://doi.org/10.1021/acsami.4c16229
ACS Appl. Mater. Interfaces 2024, 16, 65677−65686

less in cyclohexane due to higher solubility, resulting in a more homogeneous film with greater coverage at the solution interface during the initial rapid cross-linking, which instead, slows down further cross-linking. In both solvents, major pores have a radius of ∼2 Å, essential for water-salt separation. However, the cyclohexane system exhibits more subnanopores with a T-shaped structure and a slightly wider pore size distribution than the *n*-hexane system. The analyses of membrane structural properties are in agreement with previous experimental measurements regardless of several assumptions in our simulations. Our fundamental study of the IP process in an explicit solvent environment will be critical for future design of cross-linked polyamide membranes for various applications in the industry.

■ ASSOCIATED CONTENT

Supporting Information

The Supporting Information is available free of charge at https://pubs.acs.org/doi/10.1021/acsami.4c16229.

The atom types and partial charges before and after the condensation reaction in TMC and MPD, simulation parameters, snapshots of cyclohexane and *n*-hexane systems during cross-linking processes, temporal evolution of the total number of bonds formed, temporal evolution of density maps for *n*-hexane and cyclohexane systems, and two-dimensional orientation distribution $\omega(z, \theta)$ of MPD monomers at the solution interface between water and *n*-hexane or cyclohexane phases at the end of the simulations (PDF)

■ AUTHOR INFORMATION

Corresponding Authors

Benjamin S. Hsiao − *Department of Chemistry, Stony Brook University, Stony Brook, New York 11794, United States;* orcid.org/0000-0002-3180-1826; Email: benjamin.hsiao@stonybrook.edu

Tao Wei − *Department of Biomedical Engineering, University of South Carolina, Columbia, South Carolina 29208, United States; Department of Chemical Engineering, University of South Carolina, Columbia, South Carolina 29208, United States;* orcid.org/0000-0001-6888-1658; Email: taow@mailbox.sc.edu

Authors

Size Zheng − *Department of Chemistry, Stony Brook University, Stony Brook, New York 11794, United States; College of Materials and Chemistry & Chemical Engineering, Chengdu University of Technology, Chengdu, Sichuan 610059, P. R. China*

Jacob Gissinger − *Department of Chemical Engineering and Materials Science, Stevens Institute of Technology, Hoboken, New Jersey 07030, United States;* orcid.org/0000-0003-0031-044X

Complete contact information is available at: https://pubs.acs.org/10.1021/acsami.4c16229

Author Contributions

The manuscript was written through contributions of all authors. All authors have given approval to the final version of the manuscript.

Notes

The authors declare no competing financial interest.

■ ACKNOWLEDGMENTS

TW and BSH acknowledge the financial support from the NSF CBET's Interfacial Engineering program (CBET-2132524). TW and BSH are also grateful for the computational resources from the program of ACCESS (MAT230077) and the Texas Advanced Computing Center (TACC).

■ ABBREVIATIONS

IP, interfacial polymerization; MPD, phenylenediamine; TMC, trimesoyl chloride; TFC, thin film composite; MD, molecular dynamics; DPC, the degree of polymer cross-linking

■ REFERENCES

(1) Morgan, P. W. Condensation Polymers: by Interfacial and Solution Methods; Interscience Publishers, 1965.

(2) Cadotte, J. E. Evolution of Composite Reverse Osmosis Membranes. *Materials Science of Synthetic Membranes* **1985**, *269*, 273−294.

(3) Cadotte, J. E.; Petersen, R. J.; Larson, R. E.; Erickson, E. E. A new thin-film composite seawater reverse osmosis membrane. *Desalination* **1980**, *32*, 25−31.

(4) Ghosh, A. K.; Jeong, B.-H.; Huang, X.; Hoek, E. M. Impacts of reaction and curing conditions on polyamide composite reverse osmosis membrane properties. *J. Membr. Sci.* **2008**, *311*, 34−45.

(5) Tan, Z.; Chen, S.; Peng, X.; Zhang, L.; Gao, C. Polyamide membranes with nanoscale Turing structures for water purification. *Science* **2018**, *360*, 518−521.

(6) Verma, N.; Chen, L.; Fu, Q.; Wu, S.; Hsiao, B. S. Ionic Liquid-Mediated Interfacial Polymerization for Fabrication of Reverse Osmosis Membranes. *Membranes* **2022**, *12*, 1081.

(7) Liu, C.; Yang, J.; Guo, B. B.; Agarwal, S.; Greiner, A.; Xu, Z. K. Interfacial polymerization at the alkane/ionic liquid interface. *Angew. Chem.* **2021**, *133*, 14757−14764.

(8) Falca, G.; Musteata, V. E.; Chisca, S.; Hedhili, M. N.; Ong, C.; Nunes, S. P. Naturally Extracted Hydrophobic Solvent and Self-Assembly in Interfacial Polymerization. *ACS Appl. Mater. Interfaces* **2021**, *13*, 44824−44832.

(9) Habib, S.; Larson, B. E.; Weinman, S. T. Effect of surfactant structure on MPD diffusion for interfacial polymerization. *J. Membr. Sci. Lett.* **2023**, *3*, 100055.

(10) Wei, T.; Ren, C. Theoretical simulation approaches to polymer research. *Polymer science and innovative applications* **2020**, 207−228.

(11) Huang, H.; Zhang, C.; Crisci, R.; Lu, T.; Hung, H. C.; Sajib, M. S. J.; Sarker, P.; Ma, J.; Wei, T.; Jiang, S.; et al. Strong Surface Hydration and Salt Resistant Mechanism of a New Nonfouling Zwitterionic Polymer Based on Protein Stabilizer TMAO. *J. Am. Chem. Soc.* **2021**, *143*, 16786−16795.

(12) Jahan Sajib, M. S.; Wei, Y.; Mishra, A.; Zhang, L.; Nomura, K. I.; Kalia, R. K.; Vashishta, P.; Nakano, A.; Murad, S.; Wei, T. Atomistic Simulations of Biofouling and Molecular Transfer of a Cross-linked Aromatic Polyamide Membrane for Desalination. *Langmuir* **2020**, *36*, 7658−7668.

(13) Wei, T.; Zhang, L.; Zhao, H.; Ma, H.; Sajib, M. S.; Jiang, H.; Murad, S. Aromatic Polyamide Reverse-Osmosis Membrane: An Atomistic Molecular Dynamics Simulation. *J. Phys. Chem. B* **2016**, *120*, 10311−10318.

(14) Zhang, C.; Bu, G.; Sajib, M. S. J.; Meng, L.; Xu, S.; Zheng, S.; Zhang, L.; Wei, T. PXLink: A simulation program of polymer crosslinking to study of polyamide membrane. *Comput. Phys. Commun.* **2023**, *291*, 108840.

(15) Sarker, P.; Chen, G. T.; Sajib, M. S. J.; Jones, N. W.; Wei, T. Hydration and antibiofouling of TMAO-derived zwitterionic polymers surfaces studied with atomistic molecular dynamics simulations. *Colloids Surf., A* **2022**, *653*, 129943.

(16) Wei, T.; Sajib, M. S.; Samieegohar, M.; Ma, H.; Shing, K. Self-Assembled Monolayers of an Azobenzene Derivative on Silica and Their Interactions with Lysozyme. *Langmuir* **2015**, *31*, 13543−13552.

(17) Wu, Y.; Lin, T.; Santos, E.; Ahn, D.; Marson, R.; Sarker, P.; Chen, X.; Gubbels, F.; Shephard, N. E.; Mohler, C.; et al. Molecular behavior of silicone adhesive at buried polymer interface studied by molecular dynamics simulation and sum frequency generation vibrational spectroscopy. *Soft Matter* **2024**, *20*, 4765−4775.
(18) Wang, L.; He, J.; Heiranian, M.; Fan, H.; Song, L.; Li, Y.; Elimelech, M. Water transport in reverse osmosis membranes is governed by pore flow, not a solution-diffusion mechanism. *Sci. Adv.* **2023**, *9*, No. eadf8488.
(19) Xiang, Y.; Xu, R.-G.; Leng, Y. How alginate monomers contribute to organic fouling on polyamide membrane surfaces? *J. Membr. Sci.* **2022**, *643*, 120078.
(20) Liu, Y.; Zhang, D.; Tang, Y.; Gong, X.; Zheng, J. Development of a radical polymerization algorithm for molecular dynamics simulations of antifreezing hydrogels with double-network structures. *npj Comput. Mater.* **2023**, *9*, 209.
(21) Zhang, M.; Zhang, D.; Chen, H.; Zhang, Y.; Liu, Y.; Ren, B.; Zheng, J. A multiscale polymerization framework towards network structure and fracture of double-network hydrogels. *npj Comput. Mater.* **2021**, *7*, 39.
(22) Choubey, A.; Vedadi, M.; Nomura, K.-i.; Kalia, R. K.; Nakano, A.; Vashishta, P. Poration of lipid bilayers by shock-induced nanobubble collapse. *Appl. Phys. Lett.* **2011**, *98*, 023701.
(23) Kim, S. H.; Kwak, S. Y.; Suzuki, T. Positron annihilation spectroscopic evidence to demonstrate the flux-enhancement mechanism in morphology-controlled thin-film-composite (TFC) membrane. *Environ. Sci. Technol.* **2005**, *39*, 1764−1770.
(24) Fu, Q. Grazing Incidence Wide-Angle X-Ray Scattering Studies of Polyamide Thin-Film Selective Layers in Reverse Osmosis Membranes. Doctoral dissertation, State University of New York at Stony Brook, 2021.
(25) Fu, Q.; Verma, N.; Ma, H.; Medellin-Rodriguez, F. J.; Li, R.; Fukuto, M.; Stafford, C. M.; Hsiao, B. S.; Ocko, B. M. Molecular Structure of Aromatic Reverse Osmosis Polyamide Barrier Layers. *ACS Macro Lett.* **2019**, *8*, 352−356.
(26) Tao, L.; He, J.; Arbaugh, T.; McCutcheon, J. R.; Li, Y. Machine learning prediction on the fractional free volume of polymer membranes. *J. Membr. Sci.* **2023**, *665*, 121131.
(27) Li, K.; Li, S.; Liu, L.; Huang, W.; Wang, Y.; Yu, C.; Zhou, Y. Molecular dynamics simulation studies of the structure and antifouling performance of a gradient polyamide membrane. *Phys. Chem. Chem. Phys.* **2019**, *21*, 19995−20002.
(28) Zhang, N.; Chen, S.; Yang, B.; Huo, J.; Zhang, X.; Bao, J.; Ruan, X.; He, G. Effect of Hydrogen-Bonding Interaction on the Arrangement and Dynamics of Water Confined in a Polyamide Membrane: A Molecular Dynamics Simulation. *J. Phys. Chem. B* **2018**, *122*, 4719−4728.
(29) Ding, M.; Ghoufi, A.; Szymczyk, A. Molecular simulations of polyamide reverse osmosis membranes. *Desalination* **2014**, *343*, 48−53.
(30) Muscatello, J.; Müller, E.; Mostofi, A.; Sutton, A. Multiscale molecular simulations of the formation and structure of polyamide membranes created by interfacial polymerization. *J. Membr. Sci.* **2017**, *527*, 180−190.
(31) Freger, V.; Ramon, G. Z. Polyamide desalination membranes: Formation, structure, and properties. *Prog. Polym. Sci.* **2021**, *122*, 101451.
(32) Sun, Y.; Yan, M.; Li, Z.; Wang, L.; Chen, X.; Luo, S. Diffusion-Regulated Interfacial Polymerization of Hierarchically Microporous Polyamide Membranes for Permselective Gas Separations. *ACS Appl. Mater. Interfaces* **2024**, *16*, 51532−51541.
(33) Chowdhury, M. R.; Steffes, J.; Huey, B. D.; McCutcheon, J. R. 3D printed polyamide membranes for desalination. *Science* **2018**, *361*, 682−686.
(34) Jiang, C.; Zhang, L.; Li, P.; Sun, H.; Hou, Y.; Niu, Q. J. Ultrathin Film Composite Membranes Fabricated by Novel In Situ Free Interfacial Polymerization for Desalination. *ACS Appl. Mater. Interfaces* **2020**, *12*, 25304−25315.
(35) Yuan, B.; Jiang, C.; Li, P.; Sun, H.; Li, P.; Yuan, T.; Sun, H.; Niu, Q. J. Ultrathin polyamide membrane with decreased porosity designed for outstanding water-softening performance and superior antifouling properties. *ACS Appl. Mater. Interfaces* **2018**, *10*, 43057−43067.
(36) Wang, J.; Zhang, S.; Wu, P.; Shi, W.; Wang, Z.; Hu, Y. In situ surface modification of thin-film composite polyamide membrane with zwitterions for enhanced chlorine resistance and transport properties. *ACS Appl. Mater. Interfaces* **2019**, *11*, 12043−12052.
(37) Xin, R.; Jiang, B.; Ma, H.; Zhang, A.; Khan, M.; Hsiao, B. S. Highly permeable nanofibrous polyamide membranes for multi-component wastewater treatment: Exploration of multiple separation mechanism. *J. Environ. Chem. Eng.* **2024**, *12*, 111894.
(38) Cheng, C.; Li, P.; Shen, K.; Zhang, T.; Cao, X.; Wang, B.; Wang, X.; Hsiao, B. S. Integrated polyamide thin-film nanofibrous composite membrane regulated by functionalized interlayer for efficient water/isopropanol separation. *J. Membr. Sci.* **2018**, *553*, 70−81.
(39) Ding, M.; Szymczyk, A.; Ghoufi, A. On the structure and rejection of ions by a polyamide membrane in pressure-driven molecular dynamics simulations. *Desalination* **2015**, *368*, 76−80.
(40) Zhu, H.; Szymczyk, A.; Ghoufi, A. Multiscale modelling of transport in polymer-based reverse-osmosis/nanofiltration membranes: present and future. *Discovery Nano* **2024**, *19*, 91.
(41) Ghoufi, A.; Dražević, E.; Szymczyk, A. Interactions of organics within hydrated selective layer of reverse osmosis desalination membrane: A combined experimental and computational study. *Environ. Sci. Technol.* **2017**, *51*, 2714−2719.
(42) An, H.; Smith, J. W.; Ji, B.; Cotty, S.; Zhou, S.; Yao, L.; Kalutantirige, F. C.; Chen, W.; Ou, Z.; Su, X.; et al. Mechanism and performance relevance of nanomorphogenesis in polyamide films revealed by quantitative 3D imaging and machine learning. *Sci. Adv.* **2022**, *8*, No. eabk1888.
(43) Lu, D.; Ma, X.; Lu, J.; Qian, Y.; Geng, Y.; Wang, J.; Yao, Z.; Liang, L.; Sun, Z.; Liang, S.; et al. Ensemble machine learning reveals key structural and operational features governing ion selectivity of polyamide nanofiltration membranes. *Desalination* **2023**, *564*, 116748.
(44) Jeong, N.; Epsztein, R.; Wang, R.; Park, S.; Lin, S.; Tong, T. Exploring the Knowledge Attained by Machine Learning on Ion Transport across Polyamide Membranes Using Explainable Artificial Intelligence. *Environ. Sci. Technol.* **2023**, *57*, 17851−17862.
(45) Thompson, A. P.; Aktulga, H. M.; Berger, R.; Bolintineanu, D. S.; Brown, W. M.; Crozier, P. S.; in 't Veld, P. J.; Kohlmeyer, A.; Moore, S. G.; Nguyen, T. D.; et al. LAMMPS - a flexible simulation tool for particle-based materials modeling at the atomic, meso, and continuum scales. *Comput. Phys. Commun.* **2022**, *271*, 108171.
(46) Gissinger, J. R.; Jensen, B. D.; Wise, K. E. Chemical Reactions in Classical Molecular Dynamics. *Polymer* **2017**, *128*, 211−217.
(47) Gissinger, J. R.; Jensen, B. D.; Wise, K. E. REACTER: A Heuristic Method for Reactive Molecular Dynamics. *Macromolecules* **2020**, *53*, 9953−9961.
(48) Gissinger, J. R.; Jensen, B. D.; Wise, K. E. Molecular modeling of reactive systems with REACTER. *Comput. Phys. Commun.* **2024**, *304*, 109287.
(49) Gissinger, J. R.; Nikiforov, I.; Afshar, Y.; Waters, B.; Choi, M. K.; Karls, D. S.; Stukowski, A.; Im, W.; Heinz, H.; Kohlmeyer, A.; et al. Type Label Framework for Bonded Force Fields in LAMMPS. *J. Phys. Chem. B* **2024**, *128*, 3282−3297.
(50) Jorgensen, W. L.; Maxwell, D. S.; Tirado-Rives, J. Development and Testing of the OPLS All-Atom Force Field on Conformational Energetics and Properties of Organic Liquids. *J. Am. Chem. Soc.* **1996**, *118*, 11225−11236.
(51) Jorgensen, W. L.; Tirado-Rives, J. Molecular modeling of organic and biomolecular systems using BOSS and MCPRO. *J. Comput. Chem.* **2005**, *26*, 1689−1700.
(52) Song, Y.; Xu, F.; Wei, M.; Wang, Y. Water Flow inside Polyamide Reverse Osmosis Membranes: A Non-Equilibrium Molecular Dynamics Study. *J. Phys. Chem. B* **2017**, *121*, 1715−1722.

(53) Song, X.; Teuler, J.-M.; Guiga, W.; Fargues, C.; Rousseau, B. Molecular simulation of a reverse osmosis polyamide membrane layer. *In silico synthesis using different reactant concentration ratios. J. Membr. Sci.* **2022**, *643*, 120010.
(54) Behera, S.; Akkihebbal, S. K. Intrinsic kinetics of interfacial polycondensation reactions- the reaction of mPDA with TMC. *Polymer* **2020**, *210*, 122982.
(55) Nowbahar, A.; Mansard, V.; Mecca, J. M.; Paul, M.; Arrowood, T.; Squires, T. M. Measuring Interfacial Polymerization Kinetics Using Microfluidic Interferometry. *J. Am. Chem. Soc.* **2018**, *140*, 3173−3176.
(56) Behera, S.; Suresh, A. K. Kinetics of interfacial hydrolysis of an aromatic acid chloride. *Chem. Eng. Res. Des.* **2019**, *146*, 154−161.
(57) Jewett, A. I.; Stelter, D.; Lambert, J.; Saladi, S. M.; Roscioni, O. M.; Ricci, M.; Autin, L.; Maritan, M.; Bashusqeh, S. M.; Keyes, T.; et al. Moltemplate: A Tool for Coarse-Grained Modeling of Complex Biological Matter and Soft Condensed Matter Physics. *J. Mol. Biol.* **2021**, *433*, 166841.
(58) Darden, T.; York, D.; Pedersen, L. Particle mesh Ewald: An N·log(N) method for Ewald sums in large systems. *J. Chem. Phys.* **1993**, *98*, 10089−10092.
(59) Nosé, S. A unified formulation of the constant temperature molecular dynamics methods. *J. Chem. Phys.* **1984**, *81*, 511−519.
(60) Hoover, W. G. Canonical dynamics: Equilibrium phase-space distributions. *Phys. Rev. A* **1985**, *31*, 1695−1697.
(61) Nosé, S.; Klein, M. L. Constant pressure molecular dynamics for molecular systems. *Mol. Phys.* **1983**, *50*, 1055−1076.
(62) Hoover, W. G. Constant-pressure equations of motion. *Phys. Rev. A* **1986**, *34*, 2499−2500.
(63) Dennison, J. M.; Xie, X.; Murphy, C. J.; Cahill, D. G. Density, Elastic Constants, and Thermal Conductivity of Interfacially Polymerized Polyamide Films for Reverse Osmosis Membranes. *ACS Appl. Nano Mater.* **2018**, *1*, 5008−5018.
(64) Shen, L.; Hung, W.-s.; Zuo, J.; Zhang, X.; Lai, J.-Y.; Wang, Y. High-performance thin-film composite polyamide membranes developed with green ultrasound-assisted interfacial polymerization. *J. Membr. Sci.* **2019**, *570*−*571*, 112−119.
(65) Roh, I. J.; Greenberg, A. R.; Khare, V. P. Synthesis and characterization of interfacially polymerized polyamide thin films. *Desalination* **2006**, *191*, 279−290.
(66) Li, W.; Liu, X.; Li, Z.; Fane, A. G.; Deng, B. Unraveling the film-formation kinetics of interfacial polymerization via low coherence interferometry. *AlChE J.* **2020**, *66*, No. e16863.
(67) Dogangun, M.; Ohno, P. E.; Liang, D.; McGeachy, A. C.; Be, A. G.; Dalchand, N.; Li, T.; Cui, Q.; Geiger, F. M. Hydrogen-Bond Networks near Supported Lipid Bilayers from Vibrational Sum Frequency Generation Experiments and Atomistic Simulations. *J. Phys. Chem. B* **2018**, *122*, 4870−4879.
(68) Verma, N. Molecular Structural Studies of Polyamide Barrier Layers in Reverse Osmosis Membranes Using X-Ray Scattering Techniques. Doctoral dissertation, State University of New York at Stony Brook, 2022.
(69) Soldera, A.; Grohens, Y. Cooperativity in stereoregular PMMAs observed by molecular simulation. *Polymer* **2004**, *45*, 1307−1311.
(70) Behera, S.; Suresh, A. K. Kinetics of interfacial hydrolysis of an aromatic acid chloride. *Chem. Eng. Res. Des.* **2019**, *146*, 154−161.

https://doi.org/10.1021/acsami.4c16229
ACS Appl. Mater. Interfaces 2024, 16, 65677−65686